ELSEVIER

Alzheimer's & Dementia 4 (2008) S67–S76

Alzheimer's & Dementia

Differentiating Alzheimer's disease from dementia with Lewy bodies and Parkinson's disease with (+)-[^{11}C]dihydrotetrabenazine positron emission tomography

Robert A. Koeppe[a,*], Sid Gilman[b], Larry Junck[b], Kris Wernette[a,b], Kirk A. Frey[a,b]

[a]*Division of Nuclear Medicine, Department of Radiology, The University of Michigan, Ann Arbor, MI, USA*
[b]*Department of Neurology, The University of Michigan, Ann Arbor, MI, USA*

Abstract

Background: Several progressive neurologic disorders begin with cognitive decline or parkinsonism, notably Alzheimer's disease (AD), Parkinson's disease (PD), and dementia with Lewy bodies (DLB). We used positron emission tomography (PET) in attempts to differentiate these disorders.
Methods: We performed PET with (+)-[^{11}C]dihydrotetrabenazine ([^{11}C]DTBZ) to examine blood-to-brain ligand transport (K_1) and striatal monoaminergic presynaptic binding (distribution volume [DV]) in 25 DLB, 30 PD, and 25 AD patients and 57 elderly controls (NC).
Results: [^{11}C]DTBZ DV was decreased significantly in caudate nucleus, anterior putamen, and posterior putamen in DLB and PD compared with AD and NC. DLB and PD groups showed an anterior-to-posterior gradient of binding loss relative to NC, least in caudate nucleus and largest in posterior putamen. The gradient was significantly steeper in PD than DLB. Both PD and DLB showed significantly greater interhemispheric striatal binding asymmetry than NC, and PD had greater asymmetry than DLB. Cerebral cortical [^{11}C]DTBZ K_1 was decreased diffusely by 4% to 8% in PD. Larger K_1 deficits occurred in AD and DLB temporoparietal and prefrontal association cortices and posterior cingulate cortex. Greater reduction of K_1 occurred in occipital cortex in DLB than AD. Receiver operating characteristic curve analyses distinguished DLB from AD more effectively on the basis of striatal DV than occipital K_1 and distinguished DLB from PD more effectively on the basis of cerebral cortical K_1 than striatal DV patterns. Overall, 90% of cases were properly classified by combining these measures.
Conclusions: PET with [^{11}C]DTBZ can differentiate DLB from both PD and AD in a single neuroimaging study.

Keywords: Dementia with Lewy bodies; Alzheimer's disease; Parkinson's disease; Nigrostriatal projection; Vesicular monoamine transporter type-2; Positron emission tomography; Dihydrotetrabenazine

1. Introduction

Degenerative disorders associated with advancing age are common. Alzheimer's disease (AD) is the most frequent neurodegeneration, affecting approximately 10% of individuals aged 65 years or older [1,2]. Parkinson's disease (PD) is the most common neurodegenerative movement disorder, affecting about 1% of individuals aged 65 or older [3,4]. The pathophysiologic processes underlying AD and PD are as yet unproved; however, each is associated with rare, single gene, inherited causes in some families. These genetic examples provide insights into potential molecular mechanisms leading to neurodegeneration in these diseases. Although these mechanisms might not explain the pathophysiology of the great majority of sporadic cases, the molecular pathways identified in the genetic cases provide potential targets for therapeutic intervention. In familial AD, discovery of mutations leading to aberrant processing of the amyloid precursor protein (APP) offers the possibility

*Corresponding author. Tel.: 734-763-9247; Fax: 734-764-2088.
E-mail address: koeppe@umich.edu

1552-5260/08/$ – see front matter
doi:10.1016/j.jalz.2007.11.016

of new, rational therapies targeting the post-translational processing of APP and the brain retention and polymerization of pathologic APP proteolytic fragments. Similarly, in PD, many of the familial mutations arise in genes involved in the structure, processing, and degradation of α-synuclein via the proteosome, offering potential targets for novel therapeutics.

With the promise of targeted disease-modifying therapies for AD and PD, however, comes the necessity of early and accurate diagnosis, permitting therapy initiation before irreversible neuronal losses. Although clinical neurologic and extant ancillary clinical testing alone are reasonably accurate when performed longitudinally after symptom onset, the accuracy of early clinical diagnosis when symptoms first appear is optimal neither in AD nor in PD. The situation is complicated further by a third neurodegenerative disorder, dementia with Lewy bodies (DLB). This entity might arise clinically in two settings, development of parkinsonism in patients with preexisting dementia or development of dementia in patients with PD. DLB is the second most frequent cause of dementia in the elderly after AD [5].

DLB is characterized clinically by dementia, parkinsonism, fluctuating cognitive impairment, and persistent unprovoked visual hallucinations, all of which might serve to distinguish it from typical AD [6–8]. In a majority of cases studied neuropathologically, DLB occurs in association with at least some of the characteristic neuropathologic changes of AD [5]. Dementia affects at least 25% to 30% of patients with PD and can develop after the onset of parkinsonian motor symptoms or in advance of them [6–8]. In addition to presence of dementia in DLB, the parkinsonian features of DLB might sometimes be distinct from PD. Although motor signs and symptoms are asymmetrical at onset in the majority of PD patients, these features are or become symmetrical in approximately 70% of DLB patients [9].

The present study was designed to compare patients with PD, AD, and DLB to determine whether a neurochemical imaging approach might be helpful in distinguishing the entities. Prior studies have indicated the potential to distinguish AD from DLB on the basis of occipital neocortical hypometabolism of [^{18}F]fluorodeoxyglucose (FDG) or by the reduced striatal binding of (+)-[^{11}C]dihydrotetrabenazine ([^{11}C]DTBZ) in DLB [10,11]. In addition, DLB might be distinguished from PD on the basis of more symmetrical nigrostriatal lesions than in typical PD [11]. We analyzed positron emission tomography (PET) studies performed previously in two related investigations by Gilman et al [11] and Bohnen et al [12] with [^{11}C]DTBZ to examine patterns of cerebral cortical blood-to-brain ligand transport (K_1) and binding (tissue-to-blood distribution volume [DV]) to the vesicular monoamine transporter type-2 (VMAT2) in nigrostriatal projection terminals [13].

2. Methods

2.1. Subjects

Experimental procedures for the present study were approved by The University of Michigan committees regulating the participation of human subjects in research and the research use of radioactive drugs. Informed consent was obtained from all participants or their caregivers before research participation. A total of 137 subjects were evaluated, including 25 with DLB, 30 with PD, 25 with AD, and 57 normal controls (NC). The diagnosis of probable DLB was based on consensus criteria [6–8], including dementia with extrapyramidal movement abnormalities, unprovoked visual hallucinations, fluctuating mental status, and hypersensitivity to dopamine augmenting or to dopamine D2 receptor blocking medications. The DLB patients had a mean age of 73 years (range, 54 to 81 years), and 19 (76%) were male. Ten of the DLB patients had parkinsonian symptoms for 1 year or more before the onset of dementia and thus had Parkinson's disease dementia (PDD), whereas 15 had dementia preceding the onset of parkinsonian symptoms or dementia developing within 1 year after the onset of parkinsonism. The diagnosis of probable PD required a highly beneficial therapeutic response from administration of dopaminomimetic medication plus two of the following signs: tremor, rigidity, or bradykinesia [14]. The PD patients had a mean age of 65 years (range, 43 to 89 years), and 21 (70%) were male. The diagnosis of AD was based on National Institute of Neurological and Communicative Diseases and Stroke/Alzheimer's Disease and Related Disorders Association (NINCDS-ADRDA) criteria [15] and limited to subjects without the features used to establish the diagnosis of DLB. The AD patients had a mean age of 69 years (range, 52 to 85 years), and 7 (28%) were male. The comparison NC had a mean age of 63 years (range, 50 to 79 years), and 31 (54%) were male.

2.2. Clinical evaluations

All subjects were evaluated with neurologic examinations, brain structural proton magnetic resonance imaging (MRI) (including T1-, proton density-, and T2-weighted image sequences), and routine laboratory studies as appropriate to ensure accuracy of the clinical diagnosis. Blood biochemical and hematology laboratory studies in the demented subjects included a complete blood count, erythrocyte sedimentation rate, biochemical profile, urinalysis, serologic test for syphilis, thyroid function evaluation, and serum levels of vitamin B_{12} and folic acid. Results of these studies were normal or were judged to be clinically insignificant by the investigators. None of the subjects had a history of disturbances in consciousness, serious head injury, stroke, or abuse of alcohol or illicit drugs. All demented subjects had a modified Hachinski ischemic score of less than 4 [16] and no focal abnormalities on computed

tomography (CT) or MRI other than "bright spots" in T2-weighted images or mild generalized atrophy. Subjects had adequate hearing and visual acuity to complete the studies, including neuropsychological evaluations to confirm presence of dementia in the AD and DLB patients. Mean Folstein Mini-Mental State Examination [17] scores were 16 (range, 2 to 29) in the DLB patients and 17 (range, 7 to 25) in the AD patients. PD subjects and NC had no evidence of dementia detected on neurologic examination, including detailed mental status evaluations. There were no systemic diseases other than the primary neurodegenerations under study that could account for the neurologic deficits in the patient groups.

We evaluated all medications subjects were taking at the time of study, and in AD and DLB patients we ensured that dementia persisted after withdrawal of medications that might impair cognition. Patients with depressive features were included only if dementia did not reverse with antidepressants. Patients with AD were permitted to continue taking acetylcholinesterase inhibitors. Thirteen DLB patients were taking carbidopa/levodopa. Three PD patients were untreated for parkinsonism at the time of study but later exhibited symptomatic treatment responses. Of the remaining PD patients, 25 were receiving carbidopa-levodopa, 5 dopamine agonists, 9 selegiline, 2 trihexyphenidyl, and 1 tolcapone.

2.3. DTBZ PET imaging

Subjects were injected intravenously with 10 to 18 mCi (370 to 666 MBq) of (+)-[^{11}C]DTBZ containing less than 50 μg mass. DTBZ binding to VMAT2 is stereospecific [18], and the active (+)DTBZ enantiomer has an affinity constant (K_D) of approximately 1 nmol/L for the VMAT2 binding site in vitro [18]. We administered the radiotracer as a partial bolus during a period of 15 to 30 seconds (55% of the total injected dose) followed by continuous infusion of the remainder (45% of the total dose) during a period of 60 minutes, resulting in stable blood and brain regional tracer concentrations after 30 minutes [19]. A dynamic time series of brain images was acquired from each subject according to the following schedule: 4 × 30 seconds; 3 × 1 minute; 2 × 2.5 minutes; 2 × 5 minutes; and 4 × 10 minutes.

During the course of these investigations, we replaced our PET scanner; 91 subjects were studied with a Siemens/CTI ECAT Exact-47 (Siemens AG, Berlin, Germany) and 46 with a Siemens/CTI ECAT Exact HR+ scanner. All scans were acquired in 3-dimensional mode with interplane septa retracted. Measured attenuation correction was performed from a 6- to 10-minute 2-dimensional transmission scan followed by segmentation and reprojection. Scatter correction was applied in all emission scan reconstructions. After Fourier rebinning (FORE) of the 3-dimensional data into 2-dimensional data sets, we reconstructed scans with smoothing parameters that provided images from both scanners providing in-plane and axial resolution of 8.5 to 9.0 mm full-width at half-maximum. Comparability of data from the scanners was further confirmed by exploratory analysis of variance of striatal regions of interest, including diagnosis, brain region, and scanner as factors. In this analysis, the scanner effect was insignificant, and there were no significant interactions of scanner with the other factors.

2.4. DTBZ parametric maps

We constructed voxel-wise brain maps of two parameters depicting DTBZ kinetics: K_1, a parameter describing blood-to-brain tracer transport, correlating closely with the patterns of cerebral blood flow and glucose metabolism; and distribution volume ratio (DVR), a parameter proportional to the VMAT2 binding site density. To form these parametric maps, each image frame from the dynamic time series was spatially co-registered by using a rigid-body transformation to reduce effects of within-scan subject motion [20]. Next, an image proportional to K_1 (relative K_1) was obtained by summing the first 4 minutes of data from the study and expressing within-subject voxel values relative to the average of the cerebellar vermis, a region typically among the least affected in cerebral blood flow, and cerebral glucose metabolism measures in prior studies of AD, PD, and DLB.

We used a bolus plus continuous infusion protocol for [^{11}C]DTBZ injection that allows use of equilibrium analyses of VMAT2 binding without requiring arterial blood sampling [19]. Equilibrium estimates of the relative DTBZ DVR were obtained with summed data between 30 and 60 minutes after injection. DVR was calculated as the ratio of activity in each voxel to the average activity in the occipital cerebral cortex, a region known to have minimal VMAT2 binding [21,22]. A more focused estimate of specific VMAT2 binding is represented by a parameter commonly termed the binding potential [23,24], written as BP_{ND} following the notation of Innis et al [25] and representing the binding potential relative to nondisplaceable uptake. This is equivalent to DVR-1, assuming that the nonsaturable components of DTBZ DV are uniform throughout the brain and are equal to the value of total DV in the occipital cortex. The validity of these assumptions has been demonstrated previously, comparing the distributions of the pharmacologically inactive (−)-[^{11}C]DTBZ enantiomer with the active (+)-[^{11}C]DTBZ enantiomer [22].

2.5. Data analyses

After calculation of functional parametric DTBZ maps within each subject, the maps were anatomically regularized through a sequence involving reorientation to the anterior commissure–posterior commissure (AC-PC) line and linear scaling [26], followed by nonlinear deformation [27] to the reference coordinate system defined by the anatomic atlas of Talairach and Tournoux [28]. These anatomic transformations

were determined on the basis of each subject's K_1 parametric map and were then applied in parallel to that subject's DVR map as well [29]. Group-averaged K_1 and DVR maps were then constructed for qualitative visual inspection.

Data volumes of interest (VOIs) were extracted from the anatomically standardized parametric maps. We have previously digitized the anatomic atlas of Talairach and Tournoux [28] and segmented a set of 50 VOIs representing both cerebral cortical (Brodmann's areas [BAs]) and subcortical regions. Values corresponding to these VOIs were extracted from each subject's K_1 map, which had been normalized relative to cerebellar vermis. Ten aggregate cerebral cortical regions were then constructed by using volume-weighted averages of individual BA VOIs: lateral frontal (BA 44, 45, 46); medial frontal (BA 8, 9, 10); anterior cingulate (BA 24, 32); lateral temporal (BA 21, 22); medial temporal (BA 28, 34, 35, 36); inferior parietotemporal (BA 20, 37); superior parietal (BA 7, 39, 40); posterior cingulate (BA 23, 31); occipital (BA 17, 18, 19); and primary sensorimotor (BA 1, 2, 3, 4, 6) cortices.

We estimated BP_{ND} in the caudate nucleus and in the anterior and posterior putamen of each hemisphere in each subject with 3-dimensional rectangular VOIs of 4.5 mm (mediolateral) × 9 mm (anteroposterior) × 9 mm (dorsoventral) dimension. We initially placed VOIs to obtain the greatest DVR corresponding to the head of the caudate nucleus. Additional striatal VOIs were then placed 9 mm posteriorly for the anterior putamen and 18 mm posteriorly for the posterior putamen, each re-centered (mediolaterally only) to obtain the volume of greatest DVR. Two brainstem VOIs were identified, corresponding to the substantia nigra and to the dorsal raphe in the midbrain of each subject. This was accomplished by placing ellipsoidal search volumes (substantia nigra, 0.31 mL; raphe, 0.41 mL) according to the stereotaxic locations of the structures, followed by extraction of the voxel DVR values with the highest 50% binding.

We calculated total striatal BP_{ND} values as the average of caudate, anterior putamen, and posterior putamen within each cerebral hemisphere. We measured asymmetry of striatal binding as the absolute difference in regional BP_{ND} values in the right and left hemispheres divided by the mean of the two sides. An anterior-to-posterior (AP) gradient of binding was calculated as the ratio of the bilaterally averaged BP_{ND} in caudate nucleus divided by the bilaterally averaged BP_{ND} in posterior putamen.

2.6. Statistical analyses

We examined between-group differences in cerebral cortical K_1 and striatal and midbrain DVR values by analysis of variance (ANOVA) (including brain region and diagnostic group as factors) followed by Student *t* tests for pair-wise comparisons. To adjust for effects of aging in the K_1 and DVR parameters, all VOI data are presented after adjustment for subject age. The predicted age-adjusted normal values for DTBZ K_1 and BP_{ND} were based on linear regressions of $\ln(K_1)$ versus age and $\ln(BP_{ND})$ versus age, respectively, as specified in a prior collection of normal subject DTBZ PET data with a broader age range than those in the present report [12]. No significant gender effects were detected in the control subjects for either K_1 or BP_{ND} ($P > .20$ for all VOI measures), and thus, gender was not included as a factor in the analyses.

3. Results

3.1. Blood-to-brain DTBZ transport

The group-averaged relative DTBZ K_1 maps revealed the expected regional patterns of reduction involving most se-

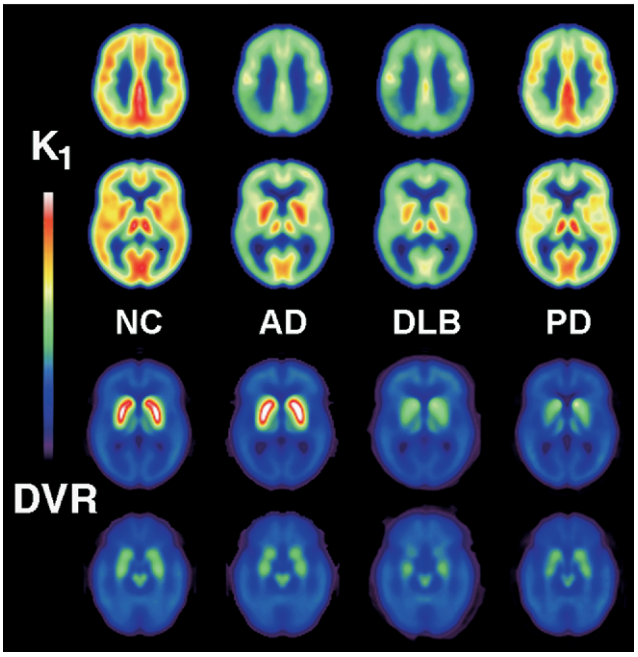

Fig 1. Transaxial slices of group mean parametric maps of [^{11}C]DTBZ relative K_1 (expressed as the within-subject ratio of K_1 voxel values to the mean of the cerebellar vermis) and VMAT2 binding (DVR) from NC (n = 57); patients with AD (n = 25); patients with DLB (n = 25); and patients with PD (n = 30). Images depict results at each of two transaxial brain levels for each parameter (AC-PC + 36 mm and + 4.5 mm for relative K_1 and AC-PC + 4.5 mm and − 9 mm for DVR). Before group averaging, each individual has been oriented with the hemisphere demonstrating lowest striatal DVR on image left. Physiologic model parameters are depicted in pseudocolor according to the lookup table at image left, with highest parameter values depicted in white and red and lowest values in blue and violet. Relative K_1 values range from 0.0 to 1.4, and DVR ranges from 0.0 to 3.0. Relative DTBZ K_1 is reduced mildly throughout the brain of PD subjects, maintaining a nearly normal pattern. Conversely, K_1 is reduced severely in AD and DLB, with most striking reductions in temporoparietal association cortex and the posterior cingulate cortex. DTBZ binding (DVR) is maintained in the AD striatum and ventral midbrain, whereas it is significantly reduced in both DLB and PD. Within the striatum, there are greater side-to-side asymmetries and greater rostrocaudal gradients of DVR deficit in PD than in DLB, as indicated by the caudate nucleus difference (image left more reduced than right) and the more severe involvement of the image left posterior putamen in PD.

verely the posterior cingulate and parietal, temporal, and prefrontal association cortices in AD and DLB (Fig. 1, top). The relative K_1 parameter was more preserved in the primary somatomotor cortex and in the basal ganglia, thalamus, and cerebellar hemispheres of AD and DLB groups. The PD group showed a mild, global decline in relative K_1 compared with NC, without disproportionate effect in any cerebral cortical area.

Age-adjusted quantification of regional cerebral cortical DTBZ K_1 demonstrated widespread, statistically significant reductions compared with controls in all three patient groups (ANOVA group-by-region interaction: f = 24.1, $P < .0001$; $df = 45$; Fig. 2). In PD, the relative K_1 values were decreased diffusely by only 4% to 8% across the regions analyzed (ANOVA group effect PD vs NC: f = 13.7, $P < .0004$). Relative cortical K_1 was significantly lower in DLB and AD than in PD in all cerebral cortical regions and was most strikingly reduced in the parietal and temporal association cortices and in the posterior cingulate cortex (mean reductions, >20% of control; ANOVA group-by-region interaction: f = 20.4, $P < .0001$; $df = 30$, AD vs DLB vs PD). Lesser relative reductions were present in anterior cingulate, medial temporal, and precentral cortices of DLB and AD groups. Differences in cerebral cortical K_1 between the AD and DLB groups were evident only in the frontal and occipital cortices (ANOVA group-by-region interaction: f = 3.35, $P < .0001$, $df = 15$, DLB vs AD). Significance thresholds (uncorrected for multiple comparisons) were $P = .021$ in the lateral frontal, .029 in the medial frontal, and .008 in the occipital cortices, respectively.

3.2. VMAT2 binding

VMAT2 binding measures were severely decreased throughout the striatum in both PD and DLB patient groups (Table 1, Fig. 1 (bottom), Fig. 3). In addition, binding was decreased in the region of the substantia nigra (ventral midbrain), but not in the nearby comparison region of midbrain raphe (dorsomedial midbrain) (Table 1, Fig. 1).

Within the striatal VOI, the pattern of involvement differed between patient groups. In NC and AD patients, the side-to-side asymmetry of striatal DTBZ BP_{ND} was significantly less than in DLB and PD patients (Table 1). Control subjects averaged an asymmetry of less than 0.04, and no individual subject exceeded an asymmetry of 0.10. AD patients averaged 0.05 asymmetry. PD patients had the greatest side-to-side asymmetry, averaging 0.17; however, this was not significantly greater than that of DLB patients (mean asymmetry, 0.10; $P = .054$ vs PD).

All three patient groups exhibited an abnormal anterior-to-posterior striatal binding gradient (Table 1). The average anterior-to-posterior gradient in controls was 0.88, whereas in the patient groups this value was larger, indicating that pathologic deficits in DTBZ binding are least in the caudate nucleus, larger in the anterior putamen, and largest in the posterior putamen. The gradient was not significantly dif-

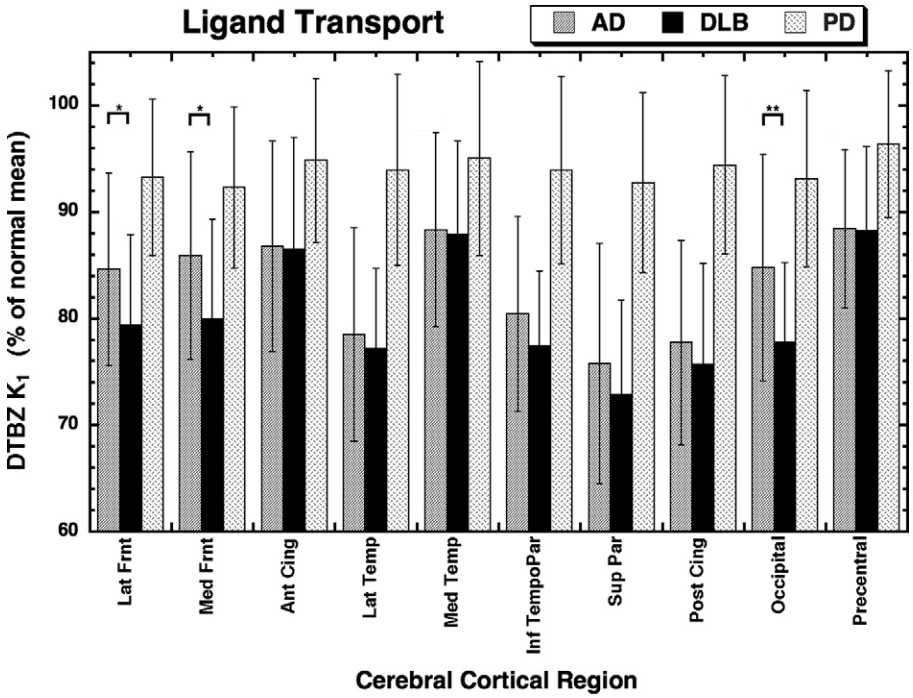

Fig 2. Age-adjusted regional cerebral cortical DTBZ K_1 values from AD, DLB, and PD patients expressed relative to control means. Error bars depict standard deviations (SD) of group measures. All cortical regions in all patient groups are significantly reduced from comparison controls. In addition, AD and DLB are significantly reduced in comparison to PD throughout the regions, with greatest distinction in the temporoparietal association cortices and in the posterior cingulate cortex. The K_1 pattern distinguishes between AD and DLB only in frontal cortices (*$P < .03$) and in the primary visual cortex (**$P < .008$).

Table 1
Striatal [^{11}C]DTBZ BP_{ND}

Region	Measure	DLB (n = 25)	PD (n = 30)	AD (n = 25)	NC (n = 57)
Caudate nucleus	DTBZ BP_{ND}	0.87 ± 0.30	0.93 ± 0.26	1.74 ± 0.35	1.69 ± 0.23
	P vs NC	8.9×10^{-15}	2.1×10^{-18}	0.24	—
	P vs AD	1.1×10^{-12}	1.7×10^{-12}	—	—
	P vs PD	0.43	—	—	—
Anterior putamen	DTBZ BP_{ND}	0.71 ± 0.25	0.65 ± 0.21	2.06 ± 0.41	2.00 ± 0.25
	P vs NC	1.7×10^{-25}	8.3×10^{-38}	0.26	—
	P vs AD	1.8×10^{-17}	1.5×10^{-15}	—	—
	P vs PD	0.40	—	—	—
Posterior putamen	DTBZ BP_{ND}	0.57 ± 0.22	0.43 ± 0.15	1.92 ± 0.42	1.91 ± 0.25
	P vs NC	7.9×10^{-30}	2.1×10^{-51}	0.46	—
	P vs AD	9.2×10^{-17}	7.9×10^{-17}	—	—
	P vs PD	0.013	—	—	—
Substantia nigra	DTBZ BP_{ND}	0.31 ± 0.13	0.27 ± 0.11	0.40 ± 0.12	0.41 ± 0.09
	P vs NC	1.9×10^{-3}	3.1×10^{-7}	0.74	—
	P vs AD	8.9×10^{-3}	9.5×10^{-3}	—	—
	P vs PD	0.23	—	—	—
Dorsal raphe	DTBZ BP_{ND}	0.39 ± 0.11	0.36 ± 0.08	0.38 ± 0.08	0.38 ± 0.08
	P vs NC	0.62	0.23	0.91	—
	P vs AD	0.30	0.17	—	—
	P vs PD	0.20	—	—	—
Striatal asymmetry	DTBZ ratio	0.10 ± 0.10	0.17 ± 0.14	0.05 ± 0.04	0.04 ± 0.03
	P vs NC	1.2×10^{-3}	8.6×10^{-6}	0.11	—
	P vs AD	7.0×10^{-3}	4.1×10^{-5}	—	—
	P vs PD	0.054	—	—	—
AP gradient (CN/PP)	DTBZ ratio	1.60 ± 0.38	2.24±0.57	0.93 ± 0.18	0.88 ± 0.08
	P vs NC	9.8×10^{-12}	5.8×10^{-19}	0.16	—
	P vs AD	1.3×10^{-9}	2.5×10^{-14}	—	—
	P vs PD	9.1×10^{-6}	—	—	—

NOTE. BP values are group means and SDs for each striatal and brainstem structure. Also shown are the interhemispheric striatal BP_{ND} asymmetry and the anteroposterior striatal BP gradient (CN/PP ratio). Two-tailed *P* values from Student *t* tests were calculated after covariation for age on the basis of a normal population of broad age range [21].

ferent between controls and AD subjects, and it was significantly steeper in both DLB and PD groups than in controls or AD subjects. The gradient was significantly greater in PD than in DLB.

3.3. Diagnostic differentiation of AD, PD, and DLB

Although the DTBZ relative K_1 and BP_{ND} measures differentiated the patient groups from the NC, even on an individual basis, some individual patient measures showed overlap between patient groups. For example, striatal BP_{ND} measures readily distinguished PD and DLB from AD and controls, but the striatal BP_{ND} pattern was only moderately effective in differentiating individual DLB subjects from PD subjects. With receiver operator characteristic (ROC) curve analyses, we assessed the robustness of criteria for distinguishing individuals across patient groups. Performance measures obtained from an ROC approach included the test sensitivity, specificity, and overall accuracy at an "optimal" test cutoff threshold. The area under the curve (AUC) serves as a comparative figure of merit for different potential tests and approaches and ranges usually from 0.5 (no discrimination ability) to 1.0 (perfect discrimination). ROC analyses for differentiation of DLB and AD (Figs. 4 and 5) demonstrated some ability to distinguish individuals on the basis of occipital cortical relative K_1 (AUC, 0.710); however, BP_{ND} was strikingly superior (AUC, 0.9936) in

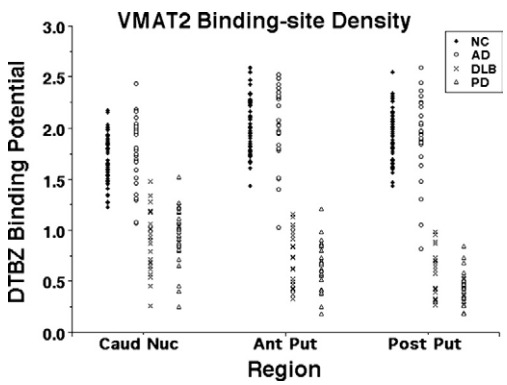

Fig 3. Striatal [^{11}C]DTBZ binding potential (BP_{ND}) values for individual subjects of each group. BP_{ND} values are shown for the bilateral average of caudate nucleus, anterior putamen, and posterior putamen regions. DTBZ binding is reduced throughout the striatal regions in PD and DLB subjects relative to NC and AD subjects, with only very minor overlap of PD and DLB values with AD. There is virtually complete overlap of values in all striatal regions between PD and DLB.

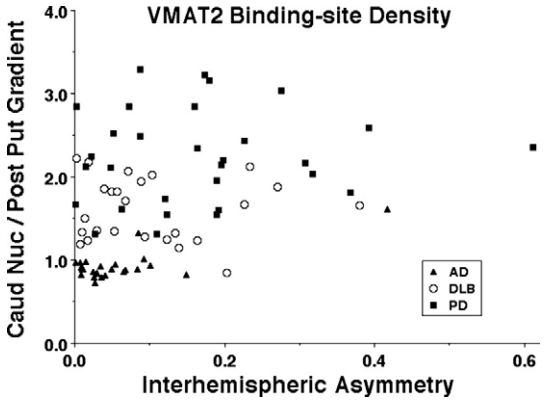

Fig 4. Interhemispheric asymmetry and anterior-posterior gradient in DTBZ binding. There are greatest levels of asymmetry and rostrocaudal gradient in the PD subjects, although there is considerable overlap of individual values between PD and DLB in both measures. AD subjects are more uniformly symmetrical and have the least rostrocaudal gradient of the patient subject groups. NC (data not shown) have minimal rostrocaudal gradients (0.884 ± 0.079) and low interhemispheric asymmetry (0.038 ± 0.026).

this distinction. Conversely, striatal BP_{ND} provided reasonable distinction between DLB and PD (Fig. 6) (AUC, 0.876), but cerebral cortical relative K_1 in the temporoparietal association cortex was far superior (AUC, 0.974). Combining both K_1 and BP_{ND} measures, with cutoff values optimized in the ROC analyses, 72 of 80 patient subjects (90.0%), as well as 54 of 57 control subjects (94.7%), were classified correctly. Individual K_1 and BP_{ND} measures expressed as a percent of the age-adjusted normal mean for all 137 subjects analyzed in this study are plotted in Fig. 7.

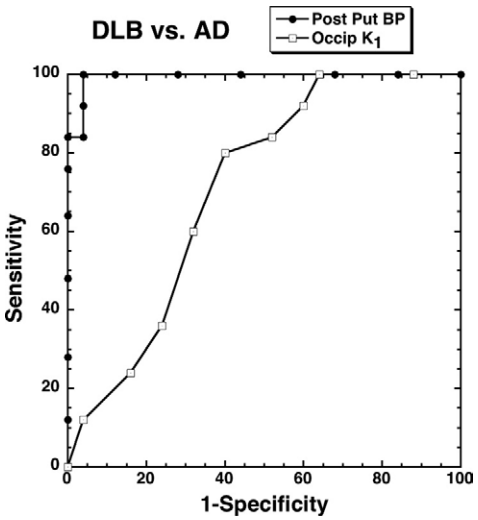

Fig 5. ROC curves depicting discrimination of DLB and AD on the basis of the most significant features of DTBZ K_1 or BP_{ND}. In relative DTBZ K_1 images, there is differential reduction in the occipital cortex of DLB (area under ROC curve, 0.710), as is reported previously in PET scans of regional cerebral glucose metabolism with FDG. There is far superior distinction of DLB and AD, however, on the basis of striatal DTBZ BP_{ND} (area under ROC curve, 0.9936). Decision threshold criteria in the K_1 ROC curve (when moving from the upper right toward lower left of the ROC curves) are the number of SDs below the normal mean and range from 1.0 to 2.5 in increments of 0.25, followed by increments of 0.5 from 2.5 to 4.0. Decision threshold criteria in the BP_{ND} ROC curve are the number of SDs different than the normal mean, ranging from 3.0 SDs above to 3.0 SDs below in increments of 1.0 and then increments of 0.5 from 3.0 to 7.0 SDs below the normal mean.

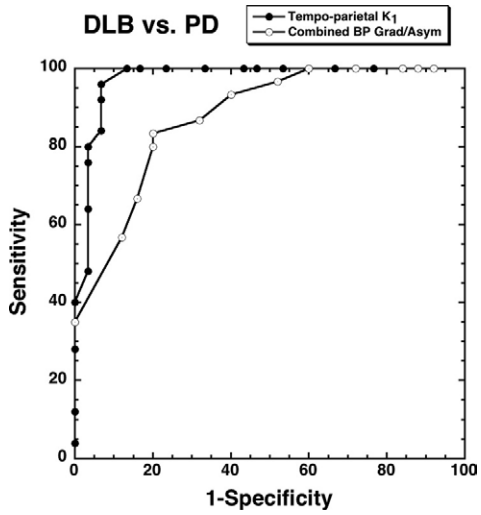

Fig 6. ROC curves for discrimination of DLB and PD on the basis of the most significant features of DTBZ K_1 or BP_{ND}. Distinction on the basis of asymmetry and rostrocaudal gradients in striatal DTBZ BP can be made on the basis of greater values in each contrast in PD subjects (area under ROC curve, 0.876). Distinction is superior for the relative K_1 parameter decrease in the temporoparietal cerebral cortex (area under ROC curve, 0.974). Decision thresholds for ROC curves based on K_1 measures (when moving from the upper right toward lower left of the ROC curves) are the number of SDs below the normal control mean and range from 0.0 to 1.75 and 2.75 to 4.5 in increments of 0.25, with finer increments of 0.1 between 1.75 and 2.75. Decision thresholds for combined gradient and asymmetry BP measures range from 1.5 to 7.5 in increments of 0.5.

4. Discussion

Analyses in the present study supported the potential of differentiating individual subjects with the most common dementias, AD, DLB, and PD without dementia, on the basis of a single neuroimaging procedure. Although we replicated prior observations that patterns of cerebral metabolism and blood flow differ between AD and DLB groups, and that the pattern of striatal dopamine denervation differs between PD and DLB groups, the sensitivity and specificity of these distinctions are not sufficient to classify individual subjects accurately. In contrast, striatal presynaptic dopaminergic innervation, assessed with [^{11}C]DTBZ DV, distinguishes AD from DLB with sufficient accuracy to classify individual subjects. Furthermore, the blood-to-brain [^{11}C]DTBZ K_1 pattern, a surrogate for the pattern of cerebral blood flow and energy metabolism, accurately distinguishes among individual subjects with PD and those with DLB. Together, these complementary neuroimaging mea-

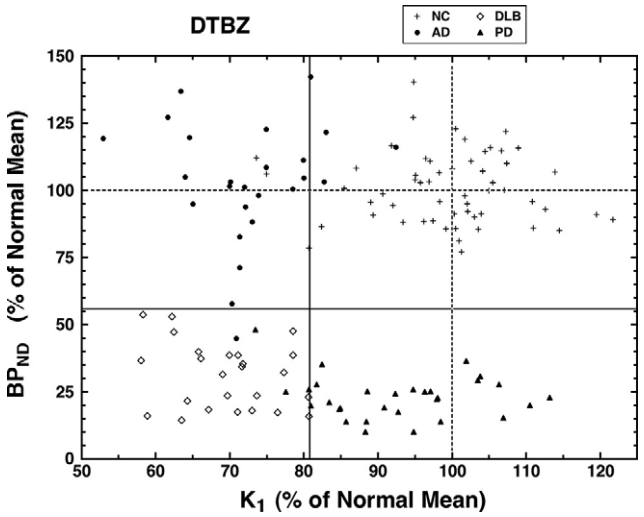

Fig 7. Discrimination of AD, DLB, and PD by using [^{11}C]DTBZ. The DTBZ VMAT2 measure (BP) distinguishes AD from DLB and PD, whereas the DTBZ blood-to-brain transport measure (K_1) distinguishes AD and DLB from PD. The solid horizontal and vertical lines demarcate the best values for diagnostic distinction as determined by the ROC analyses depicted in Figs. 5 and 6. With these two simple thresholds, 70 of 80 patients (90.0%) are categorized correctly.

surements, derived from a single neuroimaging procedure, accurately classify more than 90% of individual subjects as AD, DLB, or PD.

4.1. DLB and PDD

The emerging recognition of DLB as a frequent neurodegenerative entity and the fact that it is difficult to diagnose clinically with adequate sensitivity pose potentially important problems in both clinical management and neurodegeneration research. Three consensus conferences have been published defining DLB and supporting the notion that clinically DLB should be divided into two categories, DLB and PDD, the former applied to cases in which dementia precedes parkinsonism by at least 1 year and the latter when PD precedes dementia by at least 1 year [6–8]. There are at present, however, no neuropathologic or pathophysiologic data to indicate conclusively that DLB differs qualitatively between these two modes of onset. Consequently, in the present work, we used DLB to designate progressive dementia with concomitant nigrostriatal degeneration, irrespective of the onset order of clinical features.

Recent neuropathologic studies of PD showed that Lewy body pathology progresses as the clinical severity of PD increases. Braak et al [30] presented data from 110 neuropathologic cases, suggesting 6 progressive stages of PD on the basis of the neuroanatomic extent of Lewy body pathology (both somatic Lewy bodies and Lewy neurites). In stages 1 and 2, clinical signs of parkinsonism are not regularly observed, and Lewy pathology is limited to the medulla (particularly the motor nuclei of CN X and CN IX) and pons (raphe nuclei and the locus caeruleus). In stage 3, the midbrain (substantia nigra pars compacta), basal forebrain (nucleus basalis of Meynert), and hippocampus are involved, and clinical symptoms and signs of PD might be evident. In stages 4 through 6, there is additional Lewy pathology in limbic cortices, neocortical heteromodal association cortices, and first order motor and sensory association cortical areas, respectively. In stages 4 and higher, clinical signs of PD are recognized in the great majority of patients. This classification of disease progression is based on assessments of Lewy pathology, not on neuronal numbers and losses. Thus, the quantitative extent of neuropathology might not be captured by the staging. Of additional importance, autopsy cases were obtained from PD patients and from patients without PD diagnosis at community hospitals. Patients from specialty neurobehavioral and psychiatric clinics were excluded from this study. There is only one clinically diagnosed case of dementia included, and routine clinical assessments of cognitive function are not included in the data. The study contained only two additional cases that met Reagan pathologic criteria for AD (Braak AD stage IV/C or greater).

Other neuropathologic series have focused on DLB in subjects with dementia. In some series, three types of Lewy body distribution are recognized: brainstem, limbic (transitional), and neocortical. These correspond generally to Braak stages 3 to 6 and are associated with progressively higher prevalences of dementia ranging from 8% to 30% to 71%, respectively. In subjects with PD, Braak staging has been assessed recently in relationship to cognitive status [31,32]. In PD stages 3 and 4, the majority of subjects had abnormal Mini-Mental State Examination (MMSE) scores ($<$25), but fewer than 10% were severly impaired (MMSE $<$11). In Braak stages 5 and 6, almost all subjects had abnormal MMSE scores, and approximately 20% were severely impaired. There was significantly greater AD pathology (neurofibrillary tangles and amyloid plaques) in the more cognitively impaired subjects, but only one of 88 subjects met criteria for concomitant AD (Braak AD stage IV/C or greater). Thus, there is reasonable neuropathologic evidence that dementia in DLB might be the consequence of Lewy pathology, and that the distribution of Lewy pathology in DLB follows the pattern observed in PD. It remains to be established whether the co-presence of AD changes is independently contributory to cognitive dysfunction or decline, or whether the cognitive decline is associated with the severity of Lewy degeneration alone.

4.2. Limitations

In the present study, we have selected patients by using accepted research criteria for diagnosis and for distinguishing between groups. The subjects studied have not been followed through to autopsy; hence the study has the limitation of reliance on clinical criteria for diagnosis. Nevertheless, we have identified a single diagnostic imaging ap-

proach that might permit accurate identification of DLB, irrespective of symptomatic presentation. Previous studies have shown that VMAT2 and other presynaptic dopaminergic markers are decreased severely in PD [33] and also in DLB [11]; however, the accuracy of distinguishing DLB from PD on the basis of striatal presynaptic dopaminergic imaging is limited. In keeping with these results, the present study indicated that the interhemispheric asymmetry and rostrocaudal gradients of nigrostriatal projections were only reasonably helpful in distinguishing PD from DLB. Distinction of DLB from AD has been reported previously on the basis of cerebral blood flow and cerebral glucose metabolism imaging of the primary visual cortex [10]. Moreover, measurement of the blood-to-brain transport of DTBZ provides an excellent surrogate for cerebral cortical studies of PD, DLB, and AD by using FDG PET [33]. In the present studies, DTBZ transport in cerebral cortex was only mildly decreased in PD patients compared with NC, whereas DLB patients exhibited a pattern similar to that seen in AD. Use of both DTBZ transport and binding measures provides a highly accurate means of differentiating not only DLB, PD, or AD from normal but also in separating DLB from both PD and AD.

Acknowledgments

This work was supported in part by grants P01 NS15655, P50 AG08671, and M01 RR00042 from the U.S. National Institutes of Health. We thank Drs Roger Albin, Nancy Barbas, Norman L. Foster, Douglas Gelb, Judith Heidebrink, and R. Scott Turner for evaluating and referring patients to this study.

References

[1] Brookmeyer R, Gray S, Kawas C. Projections of Alzheimer's disease in the United States and the public health impact of delaying disease onset. Am J Public Health 1998;88:1337–42.

[2] Kukull WA, Bowen JD. Dementia epidemiology. Med Clin North Am 2002;86:573–90.

[3] Guttman M, Slaughter PM, Theriault M-E, DeBoer DP, Naylor CD. Burden of parkinsonism: a population-based study. Mov Dis 2003; 18:313–9.

[4] Strickland D, Bertoni JM. Parkinson's prevalence estimated by a state registry. Mov Dis 2004;19:318–23.

[5] Ince PG, McKeith IG. Dementia with Lewy bodies. In: Dickson DW, ed. Neurodegeneration: the molecular pathology of dementia and movement disorders. Basel: International Society of Neuropathology Press; 2003. p. 188–99.

[6] McKeith IG, Galasko D, Kosaka K, Perry EK, Dickson DW, Hansen LA, et al. Consensus guidelines for the clinical and pathologic diagnosis of dementia with Lewy bodies (DLB): report of the consortium on DLB international workshop. Neurology 1996;47:1113–24.

[7] McKeith IG, Perry EK, Perry RH. Report of the second dementia with Lewy body international workshop: diagnosis and treatment. Neurology 1999;53:902–5.

[8] McKeith IG, Dickson DW, Lowe J, Emre M, O'Brien JT, Feldman H, et al. Diagnosis and management of dementia with Lewy bodies: third report of the DLB Consortium. Neurology 2005;65:1863–72.

[9] Martí MJ, Tolosa E, Campdelacreu J. Clinical overview of the synucleinopathies. Mov Disord 2003;18(Suppl 6):S21–7.

[10] Vander Borght T, Minoshima S, Giordani B, Foster NL, Frey KA, Berent S, et al. Cerebral metabolic differences in Parkinson's and Alzheimer's diseases matched for dementia severity. J Nucl Med 1997;38:797–802.

[11] Gilman S, Koeppe RA, Little R, An H, Junck L, Giordani B, et al. Striatal monoamine terminals in Lewy body dementia and Alzheimer's disease. Ann Neurol 2004;55:774–80.

[12] Bohnen NI, Albin RL, Koeppe RA, Wernette K, Kilbourn MR, Minoshima S, et al. Positron emission tomography of striatal monoaminergic vesicular binding in normal aging and Parkinson disease. J Cereb Blood Flow Metab 2006;26:1198–212.

[13] Koeppe RA, Gilman S, Joshi A, Liu S, Little R, Junck L, et al. ^{11}C-DTBZ and ^{18}F-FDG PET measures in differentiating dementias. J Nucl Med 2005;46:936–44.

[14] Gelb DJ, Oliver E, Gilman S. Diagnostic criteria for Parkinson's disease. Arch Neurol 1999;56:33–9.

[15] McKhann G, Drachman D, Folstein M, Katzman R, Price D, Stadlan EM. Clinical diagnosis of Alzheimer's disease: report of the NINCDS-ADRDA Work Group under the auspices of Department of Health and Human Services Task Force on Alzheimer's Disease. Neurology 1984;34:939–44.

[16] Rosen WG, Terry RD, Fuld PA, Katzman R, Peck A. Pathological verification of ischemic score in differentiation of dementia. Ann Neurol 1980;7:486–8.

[17] Folstein MF, Folstein SE, McHugh PR. Mini-Mental State: a practical method for grading the state of patients for the clinician. J Psychiatric Res 1975;12:189–98.

[18] Kilbourn M, Lee L, Vander Borght T, Jewett D, Frey K. Binding of alpha-dihydrotetrabenazine to the vesicular monoamine transporter is stereospecific. Eur J Pharmacol 1995;278:249–52.

[19] Koeppe RA, Frey KA, Kume A, Albin R, Kilbourn MR, Kuhl DE. Equilibrium versus compartmental analysis for assessment of the vesicular monoamine transporter using (+)-alpha-[11C]dihydrotetrabenazine (DTBZ) and positron emission tomography. J Cereb Blood Flow Metab 1997;17:919–31.

[20] Minoshima S, Koeppe RA, Mintun MA, Berger KL, Taylor SF, Frey KA, et al. Automated detection of the intercommissural line for stereotactic localization of functional brain images. J Nucl Med 1993; 34:322–9.

[21] Vander Borght TM, Kilbourn MR, Koeppe RA, DaSilva JN, Carey JE, Kuhl DE, et al. In vivo imaging of the brain vesicular monoamine transporter. J Nucl Med 1995;36:2252–60.

[22] Koeppe RA, Frey KA, Kuhl DE, Kilbourn MR. Assessment of extrastriatal vesicular monoamine transporter binding site density using stereoisomers of [11C]dihydrotetrabenazine. J Cereb Blood Flow Metab 1999;19:1376–84.

[23] Mintun MA, Raichle ME, Kilbourn MR, Wooten GF, Welch MJ. A quantitative model for the in vivo assessment of drug binding sites with positron emission tomography. Ann Neurol 1984;15: 217–27.

[24] Lammertsma AA, Hume SP. Simplified reference tissue model for PET receptor studies. Neuroimage 1996;4:153–8.

[25] Innis RB, Cunningham VJ, Delforge J, Fujita M, Gjedde A, Gunn RN, et al. Consensus nomenclature for vivo imaging of reversibly binding radioligands. J Cereb Blood Flow Metab 2007;27:1533–9.

[26] Minoshima S, Koeppe RA, Fessler JA, Mintun MA, Berger KL, Taylor SF, et al. Integrated and automated data analysis method for neuronal activation studies using O15 water PET. In: Uemura K, Lassen NA, Jones T, Kanno I, eds. Quantification of brain function: tracer kinetics and image analysis in brain PET. Inter-

national Congress Series 1030. Tokyo: Excerpta Medica; 1993. p. 409–18.

[27] Minoshima S, Koeppe RA, Frey KA, Kuhl DE. Anatomic standardization: linear scaling and nonlinear warping of functional brain images. J Nucl Med 1994;35:1528–37.

[28] Talairach J, Tournoux P. Co-planar stereotaxic atlas of the human brain. New York: Thieme; 1988.

[29] Frey KA, Minoshima S, Koeppe RA, Kilbourn MR, Berger KL, Kuhl DE. Stereotaxic summation analysis of human cerebral benzodiazepine binding maps. J Cereb Blood Flow Metab 1996;16: 409–17.

[30] Braak H, Ghebremedhin E, Rub U, Bratzke H, Del Tredici K. Stages in the development of Parkinson's disease-related pathology. Cell Tissue Res 2004;318:121–34.

[31] Braak H, Rub U, Jansen Steur EN, Del Tredici K, de Vos RA. Cognitive status correlates with neuropathologic stage in Parkinson disease. Neurology 2005;64:1404–10.

[32] Braak H, Rub U, Del Tredici K. Cognitive decline correlates with neuropathological stage in Parkinson's disease. J Neurol Sci 2006; 248:255–8.

[33] Frey KA, Koeppe RA, Kilbourn MR. Imaging the vesicular monoamine transporter. Advances in Neurology 2001;86:237–47.